Paper No. 6a.O-11

INPUT SHAPED LARGE THRUST MANEUVER WITH A TETHERED DEBRIS OBJECT

Lee Z. Jasper and Hanspeter Schaub

6th European Conference on Space Debris

ESOC, Darmstadt, Germany April 22–25, 2013

INPUT SHAPED LARGE THRUST MANEUVER WITH A TETHERED DEBRIS OBJECT

L. Jasper and H. Schaub

Aerospace Engineering Sciences Department, University of Colorado, Boulder, CO USA, Lee.Jasper@Colorado.edu, Hanspeter.Schaub@Colorado.edu

ABSTRACT

In order to reduce the debris population in LEO, remediation is necessary. An active debris removal method is explored that utilizes fuel reserves on a recently launched upper stage to rendezvous with, and tether to, debris. The system's tethered dynamics are explored using a discretized tether model attached to six degree of freedom end bodies. The thrust output is shaped to remove the spectral energy at the natural frequencies of the tether, significantly reducing the post-burn relative motion between the vehicles. The sensitivity of the input shaping performance due to imperfect knowledge of the debris mass demonstrates that a double notch spanning multiple frequencies around the first mode is necessary to be robust to unknown debris mass. On-orbit simulations show that input shaping helps the tethered system achieve smooth oscillations about a gravity gradient alignment, reducing collision likelihood.

Key words: active debris removal, tether, input shaping.

1. INTRODUCTION

Space debris is becoming a major concern for orbital assets. While there are about 22,000 objects currently tracked, there are may thousands of dangerous debris objects in orbit[1]. In recent years, the creation of debris is on the rise, largely due to two major catastrophic events: the Fengyun 1C anti-satellite test (ASAT)[2] that created over 3300 objects[3] and the Cosmos-Iridium collision[4] that created over 1700 objects[5].

Because of these events and the continued heavy use of low Earth orbit (LEO), the debris cascade effect predicted by Kessler[6] is occurring[7]. Mitigation methods have been shown to be important, but offer only partial solutions to reducing the future debris environment. Active Debris Removal (ADR) of five or more large objects per year is shown to be an effective way to reduce the debris population[8]. Some proposed methods[9, 10, 11, 12, 13, 14] utilize harpoons, mechanical grapples, or nets to grab the debris object. While the study of the debris capture system is beyond the scope of this paper, all of these methods are likely to use tethers to connect the debris to the ADR craft to avoid close proximity operations between the tug and a tumbling object. While tethers have been studied for years[15]and actually flown on several missions[16], their use in a high force, high thrust environment has been unexplored.

To deorbit debris, the tethers must operate in short-term high stress environments during the large thrust maneuvers ($\sim$2000 N). This paper models the tether dynamics using a series of spring-mass components to discretize the tether into multiple, small masses to simulate higher order modes of the tether (similar models used in [17, 18]). The ends of the tether have two, six degree of freedom large rigid bodies: one is the ADR craft and the other is the debris. The ADR craft provides thrust that, transferred through the tether, changes the periapsis of the debris object and reduces both objects' orbital lifetimes. Ideally, the ADR craft is a rocket body with remaining fuel reserves that has recently put its payload into orbit. The remaining fuel is used to rendezvous with, and deorbit, the debris. The concept is shown in Figure 1. Depending upon initial starting altitude and amount of fuel available to the ADR craft, the debris-tug system could be deorbited within a single orbit revolution. The tethered tug-debris architecture therefore provides a cost-effective ADR system because it deorbits two pieces of potential debris for each mission.

The challenge with using a tethered tug is avoiding post-burn collision between the debris and tug. The strain put into the tether by the thrust will result in the tether pulling the two bodies towards each other post-thrust. Reducing strain and the relative motion between the bodies is necessary to remove collision potential. This paper reduces the complex on-orbit, six degree-of-freedom dynamics problem to a one-dimensional deep space scenario to analyse the challenges of implementing input-shaped thrusting on a multi-mode, tethered tug-debris system. In particular, the mass of the debris objects is not well known and the effect of this uncertainty on the post-burn relative velocity can be explored in deep space simulations. Finally, deep space is a reasonable first order assumption for approximating the dynamics of the tethered system during thrusting because the thrust maneuver only lasts a few minutes. The orbital motion and the deep space motion will not vary significantly in this time as low Earth orbits have periods around 2 hours.

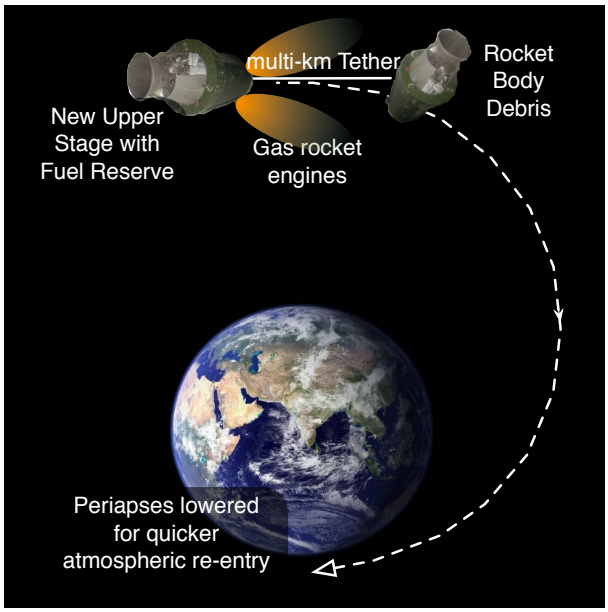

Figure 1. Tethered Tug-Debris Concept

The study also briefly investigates how the post-burn relative motion evolves if the tethered tug-debris is in LEO. Of interest is investigating how the post-burn relative velocities impact the motion over a few orbits. The tether is also assumed to be taut in this study because a slack tether results in an undesirable whipping behavior, which will not be explored in this paper. Higher order tether modes, whipping motion and end body rotation are all left to future study. Such studies warrant their own investigation because with the rotational motion of the end bodies, the tether stiffness becomes a function of the tether tension. This greatly complicates the use of input shaping techniques. Rather, the presented analysis uses a lumped mass model to set up the input-shaped maneuver, while the simulations use a higher-fidelity model which accounts for the full relative translational and rotational motion.

2. TETHER MODEL

The tether is modeled as multiple, discrete point masses. Based upon the tether material and volume the overall mass can be found. This is split into one or more, equally spaced mass particles, commonly referred to as a lumped-mass model[17, 18]. Each point mass is connected to its nearest neighbors through a spring. This is shown in Figure 2. This model allows for flexing of the tether as well as the general motion of the tether due to thrusting forces.

For this paper the tug, debris, tether, and simulation parameters are given in Table 1 and Table 2. In Table 1 the mass and inertia values for the Tug are similar to the Soyuz upper stage rocket and the debris values are

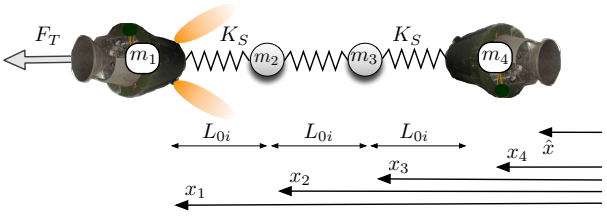

Figure 2. Tether model: Two rigid bodies, two tether point mass

close to the Cosmos-3M 2nd stage. Kevlar is used as the tether material because it is commonly used in tether analysis[19] and the diameter of 3mm is chosen to withstand the stresses experienced. In Table 2 a ∼2000 N thrust is chosen to be representative for the Soyuz upper stage thrusters while achieving the worst case, maximum tether tension, as described in Reference 11. (Note that the 'step-input' thrust linearly ramps on and off, to and from the max thrust over a period of 1 second.) The Δv capability is based upon the fuel reserves that may be available in the Soyuz after delivering a payload to orbit. Finally, the starting altitude of 800 km is based upon the known high density of Cosmos rocket bodies at that altitude and the fact that they are considered high priority targets for ADR[20].

Table 1. Vehicle Parameters

Tug Mass	2500 kg
Tug Inertia	diag[10208, 10208, 2813] kg m^2
Debris Mass	1500 kg
Debris Inertia	diag[1285, 6829, 6812] kg m^2
Tether Length	1000 m equal space between masses
Tether Material	Kevlar
Young's Modulus	1470 GPa
Tether Diameter	3 mm
Tether Cross Sectional Area	7.0686e^{-6}m^2
Tether Mass	11.822 kg[1]

Table 2. Simulation Parameters

Thrust	2009 N
Δv	100 m/s
Starting Altitude	800 km (circular)

Modeling n bodies with two rigid end-masses, $n-2$ discrete tether masses, and a spring-like tether, the equations of motion are shown in Eq. (1).

$$\dot{\boldsymbol{x}} = [A]\boldsymbol{x} + [B] \tag{1}$$

[1] http://www.matweb.com/index.aspx

where

$$\boldsymbol{x}_{2n\times 1} = \begin{bmatrix} x_1 \\ \vdots \\ x_n \\ \dot{x}_1 \\ \vdots \\ \vdots \\ \dot{x}_n \end{bmatrix} \quad [B]_{2n\times 1} = \begin{bmatrix} 0 \\ \vdots \\ 0_n \\ \frac{F_T}{m_1} \\ 0_2 \\ \vdots \\ 0_n \end{bmatrix}$$

$$[A]_{2n\times 2n} = \begin{bmatrix} & [0]_{n\times n} & & & & [I]_{n\times n} \\ -\frac{K_S}{m_i} & \frac{K_S}{m_i} & 0 & \cdots & 0_n & \\ \frac{K_S}{m_{i+1}} & -\frac{2K_S}{m_{i+1}} & \frac{K_S}{m_{i+1}} & \ddots & \vdots & \\ 0 & \ddots & \ddots & \ddots & 0_{n-2} & [0]_{n\times n} \\ \vdots & \ddots & \frac{K_S}{m_{n-1}} & -\frac{2K_S}{m_{n-1}} & \frac{K_S}{m_{n-1}} & \\ 0_n & \cdots & 0_{n-2} & \frac{K_S}{m_n} & -\frac{K_S}{m_n} & \end{bmatrix}$$

The spring constant K_S can be expressed as shown in Eq. (2).

$$K_S = \frac{EA}{L_{0_i}} \tag{2}$$

Here L_{0_i} is the initial, unstretched length of the tether between each mass, E is the Young's Modulus of Elasticity for the tether, and A is the cross sectional area. In this study, all L_{0_i} are the same. Because Eq. (1) models a tether as a spring, it is only accurate while the tether is in tension. Eq. (3) demonstrates that the tether spring force for each element is reduced to zero when there is no tension, creating an overall nonlinearity in the system.

$$T_i = \begin{cases} 0 & \text{for} \quad L_i \leq L_{0_i} \\ \frac{1}{2}K_S\Delta L_i & \text{for} \quad L_i > L_{0_i} \end{cases} \tag{3}$$

Because the tether only pulls on the masses when in tension, and does not provide a 'pushing' force when in compression, collisions between the large end-masses becomes possible. This is undesired as collisions could cause more orbital debris, something that is unacceptable from an ADR system. It therefore becomes important to study the complex tether dynamics between high-force and slack tether motion and then control those dynamics. Figure 3 demonstrates that the deep space motion simulation between the masses results in collisions. The simulation used to produce Figure 3 uses two discrete tether masses. A general bang-bang thrust profile leaves tension in the tether which pulls the masses together, causing a collision.

When thrusting, the system oscillates between zero tether tension, to high tension. This oscillation occurs at the natural frequency(ies) of the system. Therefore, one very effective way to reduce this motion, and collisions, is to remove these natural frequencies.

3. THRUSTER INPUT-SHAPING

Input shaping is a common way to remove an undesired frequency response in a linear system[21, 22]. For this specific application, a notch filter is used to remove the natural frequency of the tethered system. A brief summary of a notch filter is given for ease of reference.

In the frequency domain, a first order notch filter is defined as:

$$g(s) = \frac{s^2 + \omega_c^2}{s^2 + \text{BW}s + \omega_c^2} \tag{4}$$

where s is the frequency, ω_c is the cut-off or notch frequency, and BW is the bandwidth of the notch filter.

It is also helpful to be able to notch two frequencies at once. This is simply created by multiplying two notch filters together, in the frequency domain, that have different cut-off frequencies.

$$g(s) = \frac{(s^2 + \omega_{c1}^2)(s^2 + \omega_{c2}^2)}{(s^2 + \text{BW}_1 s + \omega_{c1}^2)(s^2 + \text{BW}_2 s + \omega_{c2}^2)} \tag{5}$$

ω_{c1} is the first cut-off or notch frequency, ω_{c2} is the second cut-off or notch frequency, and BW1 and BW2 are the bandwidths for each notch. Eq. (4) and Eq. (5) can be converted into the discrete domain and the time domain in many ways. This process is not discussed here.

In order to properly reduce motion between the tug and debris, the system's natural frequencies (Eigenvalues) must be known. Because the tether system is modeled as a linear spring when in tension, Eigenvalue analysis lends itself perfectly to this model.

Unfortunately, it becomes very difficult to analytically solve for the Eigenvalues and frequencies of the tether as more nodes are added. The Abel-Ruffini theorem demonstrates that there are no general algebraic solutions to polynomials of degree five and higher[23, 24]. This means that it is not likely that the full set of Eigenvalues for tether discretizations beyond three or four nodes is analytically achievable. However, this is not a major concern because the majority of the energy and dynamics of the system come from the first few modes, or Eigenvalues. Therefore, the primary modes of interest can be analytically computed for any system. Further, these modes will be the same, independent of the number of discretized nodes placed on the tether.

The Eigen-frequencies ω_n of a three body (single tether mass) system are:

$$\omega_n = \begin{pmatrix} 0 \\ 0 \\ \pm\sqrt{K_S Z_1 + K_S Z_2} \\ \pm\sqrt{K_S Z_3 + K_S Z_4} \end{pmatrix} \tag{6}$$

where

$$Z_1 = \frac{(m_2m_3+m_1(m_2+2m_3))}{2m_1m_2m_3}$$
$$Z_2 = \frac{\sqrt{m_1^2m_2^2-2m_1m_2^2m_3+(4m_1^2+m_2^2)m_3^2}}{2m_1m_2m_3}$$
$$Z_3 = \frac{(-2m_1m_3-m_2(m_1+m_3)}{2m_1m_2m_3}$$
$$Z_4 = \frac{\sqrt{-2m_1m_2^2m_3+m_2^2m_3^2+m_1^2(m_2^2+4m_3^2)}}{2m_1m_2m_3}$$

The repeated 0 roots relate to the DC offset present in the formulation of Eq. (1). Because Eq. (1) is formulated from the positions of the bodies, the equations naturally assume that zero tether force corresponds to separation distances between the masses that add up to the full tether length (i.e. L_0). Therefore the bodies have a constant, DC offset in their positions. The complex pair(s) in Eq. (7) represent the purely oscillatory motion, as expected from a spring-mass system. Eq. (7) has two sets of complex pairs due to the fact that a three body (single tether node) system has two modes: one from the full tether length and one the addition of the tether mass.

Again, it is interesting to note that the fundamental frequency is the same between the two-body, three-body, or four-body cases. This turns out to be (for two bodies: $m_1 = 2500$ kg, $m_2 = 1500$ kg; for three bodies: $m_1 = 2500$ kg, $m_2 = 11.82$ kg, and $m_3 = 1500$ kg, for four bodies: $m_1 = 2500$ kg, $m_{2a}+m_{2b} = 5.91+5.91 = 11.82$ kg, and $m_3 = 1500$ kg) $\omega_{n1} = .19$ Hz. The three node case also has its second mode at $\omega_{n2} = 3.43$ Hz. Therefore, these can become the notched frequencies used in the input-shaping approach.

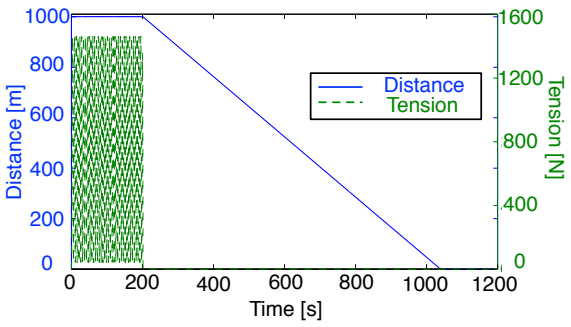

Figure 3. Relative motion and tether tension response between tug and debris for a step input 2009 N thrust, with 2 discrete tether masses

4. NUMERICAL RESULTS

4.1. Towing Results

To demonstrate why input shaping (notching) is required, consider Figure 3 where no shaping method is used during thrusting. Here the thruster cuts off at $\Delta v = 100$ m/s while there still is tension in the tether. The restoring spring force in the tether will pull all masses together and eventually cause a collision, as seen beyond 1000 s in Figure 3. It therefore becomes imperative to reduce the remaining tether tension to stop post thrust relative motion between the masses. Jasper et. al[11] demonstrate that the thrust magnitude could (based upon the tether properties and rigid body end masses) be set to achieve the desired Δv without leaving the tether in tension. This method required well known system properties and the ability to very specifically set the thrust value.

As an alternate control method, the thrust profile could include filtering so that the fundamental frequencies of the tethered system are removed. Using a notch filter (Eq. (4)), the first fundamental mode, shown in Figure 5(a) at $\omega_n = .19$ Hz, is removed and the behavior becomes much more desirable. Figure 4 and Figure 5(b) show the improvement in the post thrust dynamics. The relative motion between the tug and the first discrete tether mass is significantly reduced, shown in Figure 4 and there is less than a meter of relative drift between the two. This result is very similar for the relative motion between the other tether masses and the debris. Figure 5(b) demonstrates the dramatic difference in the response profile. The fundamental mode, seen as the first peak in Figure 5(a), is heavily attenuated in Figure 5(b).

Figure 6 compares the tether mass frequency responses. Note that this response is very similar between both tether masses modeled, therefore only one set of plots is shown. The tether masses are shown here to generally move and oscillate at higher frequencies than the larger rigid bodies. The notching has less of an effect on their behavior however there are subtle reductions in the profile below 1 Hz in Figure 6(b). Figure 7 compares the debris behavior between bang-bang and notched thrust profiles. In Figure 7(b) it is also obvious that the first mode at .19 Hz has been significantly attenuated, as desired.

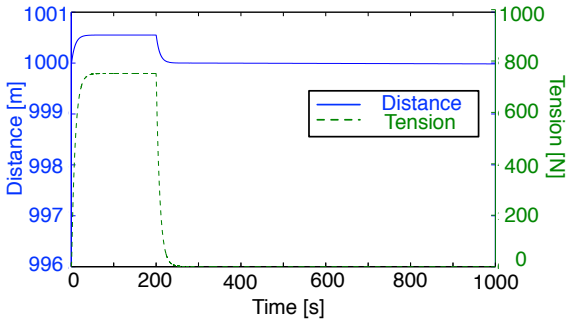

Figure 4. Relative motion and tether tension response between tug and debris for a single notch with the cut off frequency at the first mode. 2009 N thrust, with 2 discrete tether masses

4.2. Eigen-Frequency Sensitivity

The notching shown in Figure 5(b) presents an ideal case where all system parameters are well known. However, if

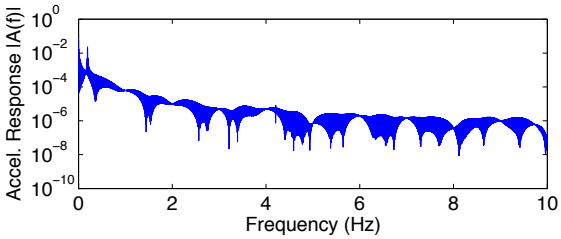

(a) Step-input thrust profile

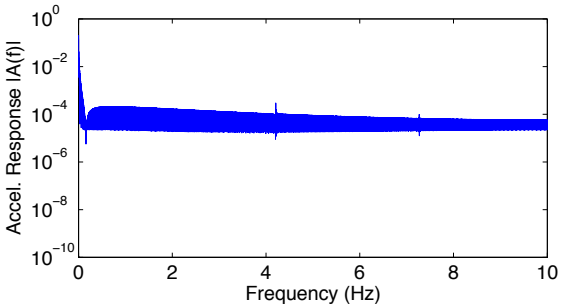

(b) Notch at $\omega_c = .19$Hz

Figure 5. Tug vehicle frequency response to 2009 N thrust, with 2 discrete tether masses

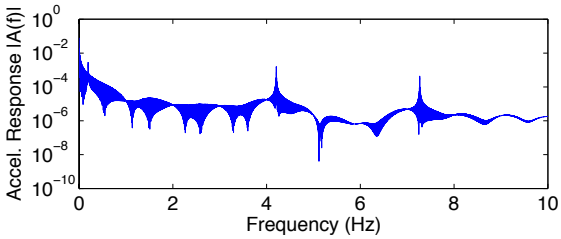

(a) Step-input thrust profile

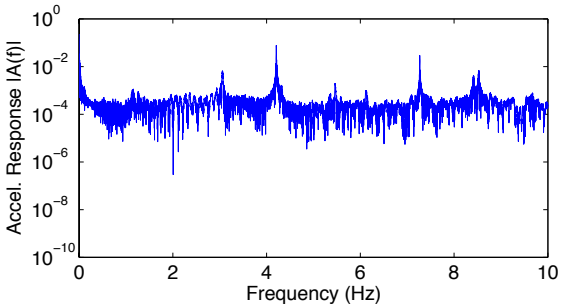

(b) Notch at $\omega_c = .19$Hz

Figure 6. Tether mass frequency response to 2009 N thrust, with 2 discrete tether masses

the Eigenvalues in Eq. (7) are not well known, the natural frequencies can change from what is expected, lowering the effectiveness of the notch filter. The debris mass (m_3 in Eq. (7)) will be the least well known value in the computations. The linear sensitivity of the natural frequency in Eq. (7) can be found by taking the partial of the natural frequency with respect to m_3 and evaluating at the expected values (given in Table 1, where the expected debris mass $m_{3e} = 1500$ kg). Eq. (7), shows the linear change in the natural frequency given the true debris mass m_{3t}.

$$\Delta\omega_n(m_{3t}) = \left.\frac{\partial\omega_n}{\partial m_3}\right|_{K_S,m_1,m_2,m_{3e}} (m_{3t} - m_{3e}) \quad (7)$$

Evaluating Eq. (7) from $m_{3t} = 600 - 2400$ kg, Figure 8 shows that the mass of the debris can vary by 900 kg (60%) and it will only change the first mode by .03 Hz. Because the first mode contains the most energy for the system this mode will be focused on. Given the tether properties, masses of the tug and debris, the first mode should occur near .19 Hz. It turns out that a variance of .03 Hz in the first mode is enough to cause the notch filter to have significant performance problems. One robust method to avoid sensitivity issues is to add a second notch in the region of the first mode.

To design a double notch around the first mode, Figure 8 is used to determine the potential range over which the first mode can vary. When two notches are placed near each other, they effectively attenuate a range of frequencies. This behavior can be seen in Figure 9 where frequencies .14 Hz – .22 Hz are very heavily notched. While there is reduced attenuation between these two frequencies it is still very large, peaking near -58 dB. This is sufficient to reduce the first mode's energy.

Using this type of double notch while including errors in debris mass knowledge, significant reductions in relative motion are still produced (Figure 10). Figure 10(a) shows that the single notch placed at the expected, but incorrect, natural frequency experiences small but noticeable collapse of the system. Conversely, Figure 10(b) shows that the double notch effectively reduces the motion between the masses, even though the exact natural frequency is not well known. It turns out that the relative motion of the masses are reduced nearly as well as the perfect single notch of Figure 4. The performance difference between the single notch and the double notch spanning a wide range of frequencies can be seen in Figure 11. The double notch experiences more attenuation of the first mode. The double notch frequency response does see less attenuation near .2 Hz, in the same location as the 'hump' in Figure 9, which is expected.

Notching does cause phase lag in the thrust profiles and the system responses. Therefore the thrust period of a step input is shorter than a single or double notch. This behavior is shown in Figure 12. It takes the step input (no shaping) about 201 seconds to achieve a $\Delta v = 100$ m/s while the single notch takes 238 seconds and the double notch 283 seconds to reach within about 1% of a 0 N thrust. This means that it takes less than five minutes for any of these methods to perform their burn, a time duration which is very short when considering an orbital period around 90 minutes in LEO.

This demonstrates that the double notch spanning the possible range of the first mode can effectively reduce collision potential between the masses with large uncertainties in the debris mass. This also demonstrates that

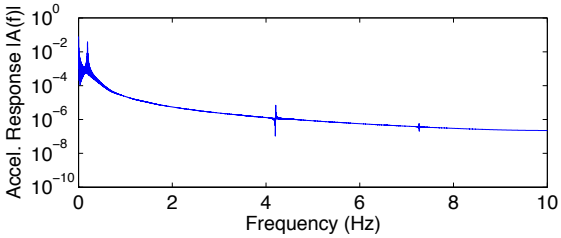

(a) Step-input thrust profile

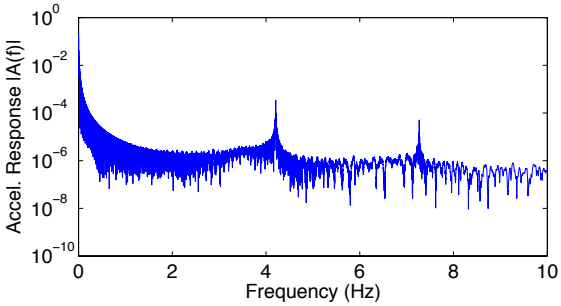

(b) Notch at $\omega_c = .19$Hz

Figure 7. Debris object frequency response to 2009 N thrust, with 2 discrete tether masses

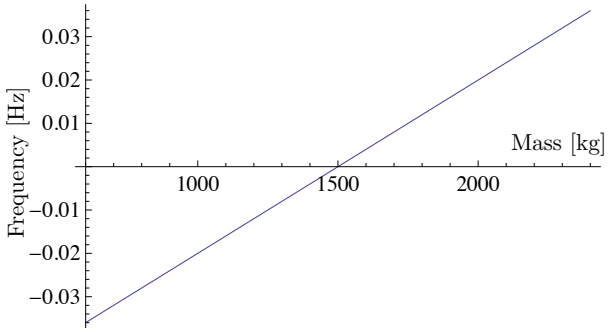

Figure 8. Sensitivity of the tether-mass system's first fundamental mode ($\omega_n = .19$ Hz) to imperfect debris mass knowledge

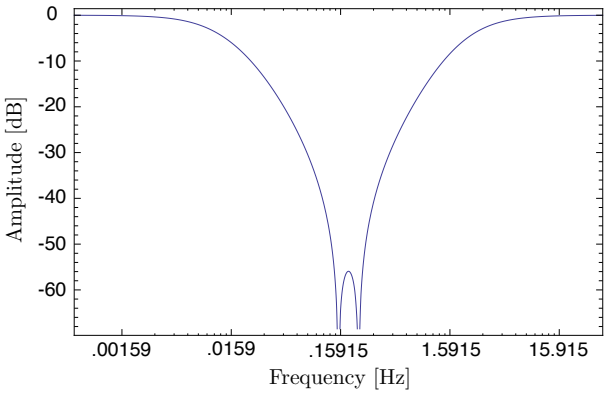

Figure 9. Double notch centered about first fundamental mode of system

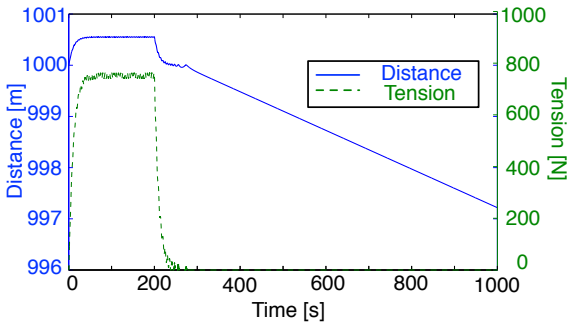

(a) Single notch, $\omega_c = .17$Hz

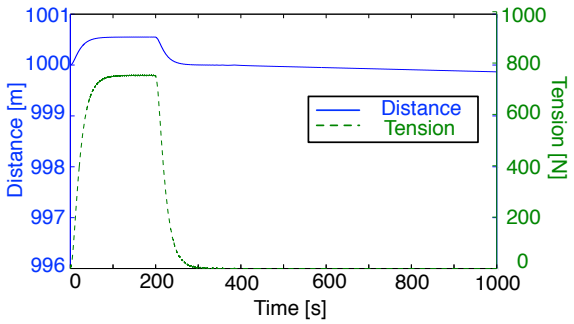

(b) Double notch spanning $.14 \leq \omega_c \leq .22$Hz

Figure 10. Relative motion and tether tension response between tug and debris for an expected debris mass of 2000 kg ($\omega_n = .17$ Hz), actual mass is 1500 kg ($\omega_n = .19$ Hz). 2009 N thrust, with 2 discrete tether masses

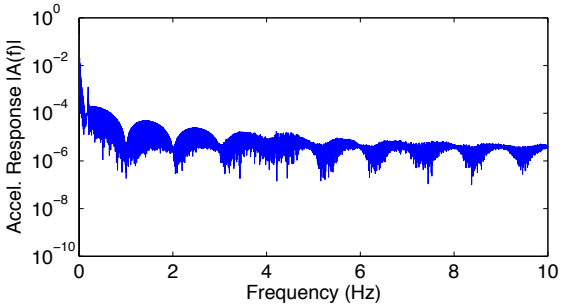

(a) Single notch, $\omega_c = .17$Hz

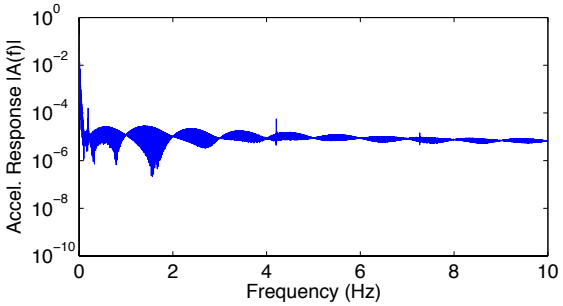

(b) Double notch spanning $.14 \leq \omega_c \leq .22$Hz

Figure 11. Tug vehicle frequency response with 2 discrete tether masses. Expected $\omega_n = .17$ Hz, actual $\omega_n = .19$ Hz

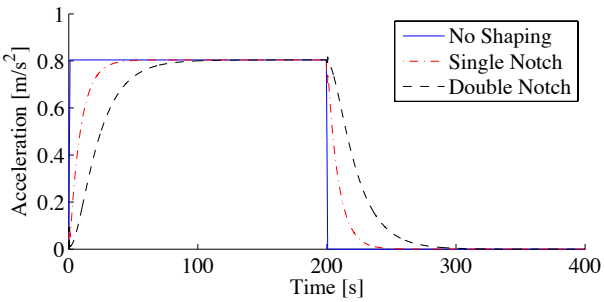

Figure 12. Thrust profiles with different input shaping techniques

the first mode is the most important and should be the focus of reducing relative motion between objects that are tethered. What is truly significant about determining that the first mode is really the only mode that needs to be notched is that this is the most simple mode to model and analyze. While tether models can become very complex (using partial differential equations and finite element solvers) the first mode is the only mode that really needs to be considered. This may help to drastically reduce the analysis required for a tether-tug system.

5. ON-ORBIT THRUST NOTCHING

To show the effectiveness of this method when on-orbit, a four mass (two tether mass) system is used with a double notch spanning across the first mode as shown in Figure 9. While the system's actual natural frequency is .19 Hz, the double notch allows for uncertainties in debris mass knowledge. The debris and tug craft are started in an 800 km circular orbit and a burn is produced in the anti-velocity direction to lower both object's orbits. A $\Delta v = 100$ m/s lowers the periapsis to about 425 km.

The double notch in Figure 13(b) experiences separation distances that are just as small as the step-input thrust of Figure 13(a) which is unexpected from the deep space simulations. However, there are several new advantages to input shaping that are not apparent in the deep space simulations. The step input system tumbles but the notched system quickly settles into a gravity gradient type configuration where the masses have aligned along the radial vector, and after one orbit, remain about the full tether length apart from each other. The notched system's oscillation about the radial vector (a nadir alignment) is shown in Figure 14 where the notched motion oscillates about 90 degrees from the in-track direction. Conversely, the step input only experiences tumbling with a large range of separation distances between the bodies. The fact that the notched system achieves a gravity gradient orientation is very encouraging and would help to keep these masses separated for their orbital lifetime. It is also encouraging to note that the tether tension forces are noticeably reduced in Figure 13(b) placing less stress on the entire system.

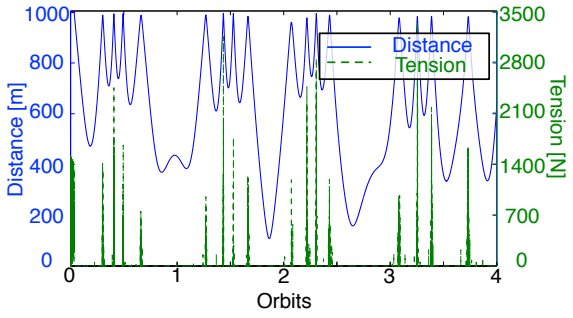

(a) Step-input thrust profile

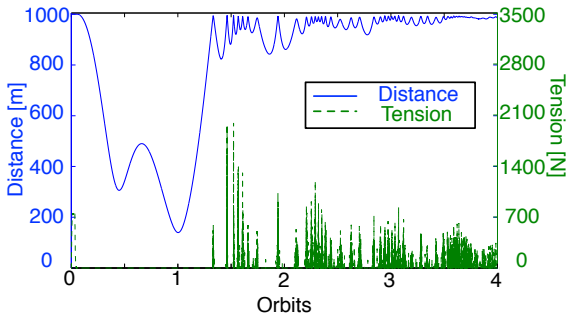

(b) Double notch spanning $.14 \leq \omega_c \leq .22$Hz

Figure 13. Relative motion and tether tension response between tug and debris for four orbits. Tether $\omega_n = .19$ Hz. 2009 N thrust, with 2 discrete tether masses

6. CONCLUSIONS

A second stage rocket body with fuel reserves could be used as an ADR system. With a tether as an energy transfer mechanism and a thrust applied by the rocket, the periapses of both objects can be significantly lowered. This allows for drag to affect their orbits more, reducing lifetimes. Step input (impulsive) thrust profiles were shown to be challenging for a tethered ADR system due to the chaotic motion, collision potential, and high tether tensions induced. It was shown that the majority of the relative motion that occurred between both craft is due to the tether's first fundamental mode. Reducing energy in-

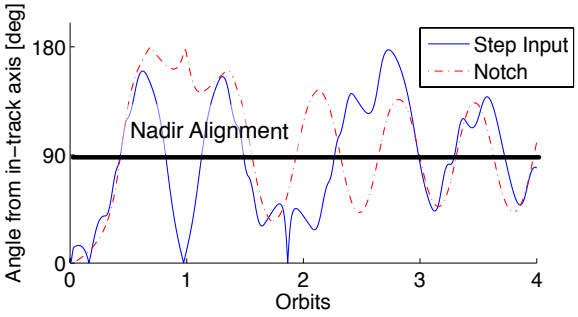

Figure 14. Angle from along-track vector. 90^o is the radial vector

put into the system at this frequency, through thrust input shaping, effectively reduced these problems. It was also shown that the first mode of the tethered system is the most important to reduce frequency input. This is very encouraging because this mode is only affected by the tether material properties and length, not the number of discretized masses or any other variable property. This means that the tether motion can be effectively modeled and studied without incredibly high-fidelity tools.

Input shaping while on-orbit results in the masses achieving a gravity gradient-like formation which will allow for separation distances to be maintained between bodies. This is very encouraging and future work may consider a tether with damping and longer lengths of tether to achieve more stable gravity gradient orientations. It is therefore likely that this type of ADR system would be practical to design and implement on-orbit.

ACKNOWLEDGMENTS

The authors would like to acknowledge Valery Trushkyakov, Professor in the Department of Aviation and Rocket Building, Omsk State Technical University for his contributions to the tethered rocket body ADR method.

REFERENCES

1. Stansbery E., (2012). *NASA Orbital Debris Program Office Frequently Asked Questions*, NASA Lyndon B. Johnson Space Center Houston, Texas
2. Pardini C., Anselmo L., (2007). Evolution of the debris cloud generated by the Fengyun-1C fragmentation event, *20th International Symposium on Space Flight Dynamics*, Goddard Space Flight Center Greenbelt, MD, NASA CP-2007-214158.
3. Kelso T., (2012). *CelesTrak. CSSI Center for Space Standards and Innovation*, http://celestrak.com/
4. Johnson N. L., (2010). Orbital Debris: The Growing Threat to Space Operations, *33rd Annual AAS Guidance and Control Conference, Breckenridge, CO*
5. Pardini C., Anselmo L., (2011). Physical properties and long-term evolution of the debris clouds produced by two catastrophic collisions in Earth orbit, *Advances in Space Research*, **48**, 557–569
6. Kessler D. J., Cour-Palais B. G., (1978). Collision Frequency of Artificial Satellites: The Creation of a Debris Belt, *Geophysical Research*, **83**(A6), 2637–2646
7. Liou J.-C., Johnson N. L., (2006). Risks in space for orbiting debris, *Science*, **311**, 340–341
8. Liou J.-C., Johnson N. L., Hill N., (2010). Controlling the growth of future LEO debris populations with active debris removal, *Acta Astronautica*, **66**(5-6) 648–653
9. Alary D., (2012). Astrium's views on OOS & ADR, *European On-Orbit Satellite Servicing and Active Debris Removal Conference, Brussels, Belgium*
10. Bonnal C., Koppel C. R., (2012). Getting rid of large debris: a safe low cost alternative, *2nd European Workshop on Active Debris Removal, Quentin, Paris, France*, paper 3.2
11. Jasper L., Schaub H., Seubert C., Trushlyakov V., Yutkin E., (2012). Tethered Tug for Large Low Earth Orbit Debris Removal, *AAS/AIAA Astrodynamics Specialists Conference, Charleston, SC*, No. AAS 12-252
12. Reed J., Busquets J., White C., (2012). Grappling System for Capturing Heavy Space Debris, *2nd European Workshop on Active Debris Removal, Quentin, Paris, France*, paper 4.2
13. Retat I., Bischof B., Starke J., Froth WP., Bennell K., (2012). Net Capture System, *2nd European Workshop on Active Debris Removal, Quentin, Paris, France*, paper 4.3
14. Trushlyakov V., Makarov J., Raykunov G., Shatrov J., Baranovo D., (2012). The development of autonomous onboard systems for the controlled deorbiting of stages separating parts of space launch vehicle, *2nd European Workshop on Active Debris Removal, Quentin, Paris, France*, paper 2.5
15. Cartmell M. P., McKenzie D. J., (2008). A Review of Space Tether Research, *Elsevier Progress in Aerospace Sciences*, **44**, 1–21.
16. Cosmo M., Lorenzini E., (1997). *Tetheres in Space Handbook*, Smithsonian Astrophysical Observatory, Prepared for NASA Marshall Space Flight Center, Cambridge, MA, ed. 3
17. Kim M., Hall C. D., (2003). Control of a rotating variable-length tethered system, *Advances in the Astronautical Sciences*, **114**, 1713–1732.
18. Williams, P., (2009). Dynamic multibody modeling for tethered space elevators, *Acta Astronautica*, **65**, 399–422.
19. Carroll J. A., Oldson J. C., (1995). Tethers for Small Satellite Applications, *AIAA/USU Small Satellite Conference, Logan, Utah*
20. Liou J.-C., (2011). An active debris removal parametric study for LEO environment remediation, *Advances in Space Research*, **47**(11), 1865–1876
21. Singhose W. E., Banerjee A. K., Seering W. P., (1997). Slewing Flexible Spacecraft with Deflection-Limiting Input Shaping, *Journal of Guidance, Control, and Dynamics*, *20*(2), 291–298
22. Lewis D., Parker G. G., Driessen B., Robinett R. D, (1999). Comparison of Command Shaping Controllers for Suppressing Payload Sway in a Rotary Boom Crane, *International Conference on Control Applications Kohala Coast Hawaii*, 719–724
23. Ore O., (1957). *Niels Henrik Abel: Mathematician Extraordinary*, U of Minnesota Press, ed. 1
24. Ayoub R. G., (1980). Paolo Ruffinis contributions to the quintic, *Archive for History of Exact Sciences*, *23*(3), 253–277